A 2D level set finite element grain coarsening study with heterogeneous grain boundary energies

Julien Fausty, Nathalie Bozzolo, Marc Bernacki

Version of Record: https://www.sciencedirect.com/science/article/pii/S0307904X19305967
Manuscript_c6788a5c1debb9e88aa9eb8552969480

A 2D Level Set Finite Element Grain Coarsening Study with Heterogeneous Grain Boundary Energies

Julien Fausty*, Nathalie Bozzolo, Marc Bernacki

MINES ParisTech, PSL Research University, Centre de mise en forme des matériaux (CEMEF), CNRS UMR 7635, CS 10207 rue Claude Daunesse, 06904 Sophia Antipolis Cedex, France

Abstract

In a previous article (Fausty et al. A novel level-set finite element formulation for grain growth with heterogeneous grain boundary energies, Materials and Design 2018; 160:578-590) a new level-set finite element formulation for pure grain growth with heterogeneous grain boundary energies (i.e. one energy per grain interface) was developed and validated for simple configurations. In this work, the authors apply this new tool to the simulation of two dimensional grain growth of polycrystals using different disorientation dependent grain boundary energy functions. The results of these full-field calculations are assessed using the time dependent evolution of the following criteria: grain size, grain number, total interface energy, grain boundary disorientation distribution, grain boundary energy distribution and number of neighboring grains distribution. Of particular interest is the relationship between the grain boundary energy function and the evolution of the grain boundary network in the sense of both its morphology and its constitution. Some notable results are that the disorientation distribution evolution is inversely correlated to the grain boundary energy function itself and that the kinetics of grain growth are heavily effected by the heterogeneity of the system.

Keywords: polycrystal, grain growth, heterogeneous grain boundary energies, finite element, level set

Email addresses: julien.fausty@mines-paristech.fr (Julien Fausty*), nathalie.bozzolo@mines-paristech.fr (Nathalie Bozzolo), marc.bernacki@mines-paristech.fr (Marc Bernacki)

Most full-field grain coarsening models have the capacity to account for the local geometry of the grain boundary network at the microstructural level [1–5]. However, there are fewer numerical tools that allow for the prediction of the time evolution of local grain boundary properties or even distributions of grain boundary characters [6–16]. Of particular note is the relatively new phase-field formulation used in [6], which allows for both the definition of heterogeneous grain boundary energies and mobilities, and the method applied in [7], which shows very interesting results in special dual grain boundary microstructures. However, in general, phase-field formulations suffer from inherent numerical instabilities when increasing the heterogeneity of the system if one does not include higher order terms [17]. Level-set methods also exist to model grain growth with heterogeneous grain boundary energies, of which the most mature is probably the one developed in [13]. Even so, the formulation in [13] uses a synthetic treatment and definition of the grain boundary energies. In this formulation, one defines a grain component energy per grain and then calculates the grain boundary energy as a linear combination of adjacent grain component energies. Other very recent work [16] goes so far as to simulate the full anisotropic case (misorientation and inclination dependent grain boundary energy) using a level-set formulation close to the one studied here [18] but on a regular grid.

In practice, the grain boundary energy function is very difficult, perhaps even impossible, to measure directly. However, aspects of the function itself may be parameterized through experimental studies of grain boundary movement. Often when experimentalists look to use a homogeneous grain boundary energy model, they first look at the kinetics of pure grain growth in their material [19, 20]. Using a Burke-Turnbull type law, they can deduct an approximated value for the reduced mobility.

Implicit in this work is the idea that perhaps the same could be done for determining richer models for the grain boundary energy. This model, although much simpler than the reality of a 5 parameter grain boundary model, does inversely correlate the grain boundary energy function with the disorientation distribution. This observation lends weight to the idea that aspects of the grain boundary energy dependence on the disorientation angle can be inferred from the disorientation distributions of real microstructures that have been annealed for long times. As such, if one adopts the hypotheses and simplifications that are made in the elaboration of this framework, then one could possibly use an inverse analysis approach on the disorientation distribution evolution of real materials to generate plausible candidates for

disorientation dependent grain boundary energy functions.

In the following, the level-set finite element (FE) formulation for grain coarsening [2] with heterogeneous grain boundary energies developed in [18] will be used to simulate 2D grain growth of digital polycrystals. The sensitivity of the method to both mesh size and time step will be explored. Furthermore, the variation in the evolution of a polycrystal with different forms for the grain boundary energy function will be studied. However, grain boundary energies that depend on the inclination of the grain boundaries will not be studied here because these types of energies constitute the limitations of the framework. The inclination dependent energies can be referred to as "anisotropic" while the term "heterogeneous" will be used to refer to grain boundary energies that are only misorientation dependent.

1. The numerical framework

While [18] gives a more detailed description of the framework from both a numerical and mathematical point of view, the most important aspects of the method are summarized in the following paragraphs.

1.1. The level-set method

First described in [21] the level-set method is a versatile and robust approach for modeling interface dynamics. Applicable in a number of physical problems, it was first employed for the simulation of polycrystal grain coarsening in [22]. The concept is the following: by defining a continuous scalar field ϕ in space Ω

$$\left\{ \begin{array}{cc} \phi : \Omega \to \mathbb{R} & \\ \phi(X \in \Omega) = 0 & \rightleftharpoons \quad X \in \Gamma \end{array} \right\}, \tag{1}$$

where the iso-zero value of this field represents an interface Γ, one may successfully capture the dynamics of the interface by studying the evolution of the field. This field is called a level-set. The Γ interface may be subjected to an arbitrary velocity field $\mathbf{v}$ by solving the transport equation:

$$\frac{\partial \phi}{\partial t} + \mathbf{v} \cdot \nabla \phi = 0. \tag{2}$$

As such, the models for the physical phenomena that provoke interface movement are completely encapsulated in the $\mathbf{v}$ velocity field. When the

physical space is comprised of a massively interconnected network of interfaces (as is the case in polycrystals), one may define a set of level-set functions $\Phi = \{\phi_i,\ i = \{0, \ldots, N\}\}$ that capture all the interfaces of the domain. A reciprocal set of transport equations must then be solved in order to capture the dynamics of all the interfaces. If the normalization constraint

$$|\nabla \phi| = 1 \tag{3}$$

is fulfilled $\forall x \in \Omega$, then the level-set field becomes a distance field to the Γ interface. This distance property is usually imposed in practice [2].

Often the velocity field $\mathbf{v}$ does not preserve the space-filling property or the impenetrability constraints of the level-set description of the grains of a polycrystal. The level sets flow into each other or leave voids behind. Also, the solving of the transport equation does not retain the normalization of the fields required in equation (3). As such, the resolution of

$$\phi_i(X) = \frac{1}{2}\left[\phi_i(X) - \max_{j \neq i} \phi_j(X)\right], \quad \forall i = \{0, \ldots, N\}, \tag{4}$$

is classically used [22] to correct both overlaps and voids in the microstructure and a direct re-initialization procedure [23] is used to re-normalize the gradient of the level-set functions after solving the transport equations.

1.2. The grain boundary velocity formulation

The velocity field $\mathbf{v}$ is the object through which the physics of grain coarsening is introduced to the simulation. For various reasons described in [18] the expression used in this work for the velocity of the grain boundary is

$$\mathbf{v} = \mu(\nabla \gamma \cdot \mathbf{n} - \gamma \kappa)\mathbf{n}, \tag{5}$$

where μ is the mobility of the grain boundary, γ is the energy of the grain boundary, $\mathbf{n}$ is the outside normal to the grain boundary and κ is the mean curvature of the grain boundary. This formulation has been developed in an isochoric and isothermal setting where no other defects beyond the grain boundaries are present in the microstructure. These same assumptions are applied here. If the level-set function ϕ used to describe a grain is a distance

function, positive inside the grain and negative outside, then

$$\mathbf{n} = -\nabla\phi(X \in \Gamma), \tag{6}$$
$$\kappa = -\Delta\phi(X \in \Gamma), \tag{7}$$

and as such

$$\mathbf{v} = \mu(\nabla\gamma \cdot \nabla\phi - \gamma\Delta\phi)\nabla\phi \tag{8}$$

which leads to a strong formulation of the transport equation (2)

$$\frac{\partial\phi}{\partial t} + \mu\nabla\gamma \cdot \nabla\phi - \gamma\Delta\phi = 0 \tag{9}$$

and the weak formulation, with $\varphi \in H_0^1(\Omega)$,

$$\int_\Omega \frac{\partial\phi_i}{\partial t}\varphi d\Omega + 2\int_\Omega \mu\nabla\gamma \cdot \nabla\phi_i\varphi d\Omega + \int_\Omega \mu\gamma\nabla\varphi \cdot \nabla\phi_i d\Omega - \int_{\partial\Omega} \mu\gamma\varphi\nabla\phi_i \cdot n_{\partial\Omega} d(\partial\Omega) = 0.$$

which will be referred to as the heterogeneous formulation for grain growth.

In the following, the discretized FE formulation utilizes P1 type elements with an unstructured triangular mesh and is stabilized by a streamline upwind Petrov-Galerkin method [24]. While periodic boundary conditions might be more relevant for these types of numerical simulations, both the remeshing algorithm and microstructure generation algorithm do not support the constraints of these types of boundary conditions. As such, given the usefulness of both these algorithms, von Neumann type boundary conditions are employed for the resolution of the equations which impose that the grain boundaries touching the borders of the domain be orthogonal to them locally. All the initial meshes were generated using the Gmsh software package [25].

2. Characterization of the numerical microstructure

A reference numerical microstructure will be used for the following sections. This polycrystal is representative of a monophase material with a log-normal distribution of grain sizes as shown in Figure 1.

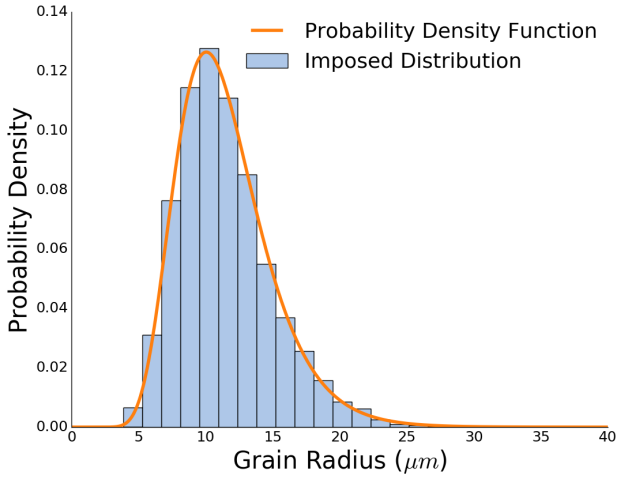

Figure 1: Normalized numerical microstructure initial grain radius distribution in both analytical form as well as discretized.

Crystallographic orientations are attributed to the grains by generating Euler angles randomly, for example Figure 2a where the color scheme is developed using the vector magnitude $e = \sqrt{\varphi_1^2 + \Phi^2 + \varphi_2^2}$ where $(\varphi_1, \Phi, \varphi_2)$ are Euler angles, leading to a Mackenzie type disorientation distribution [26] as demonstrated in Figure 2b. The computation of these disorientation angles is undertaken in exactly the same manner as in [18]. Also, all the disorientation distributions measured in this work are weighted by boundary length and not by number.

The polycrystal is generated using a Laguerre-Voronoi tessellation with a dense sphere packing algorithm described in [27]. The size of the domain determines the number of grains. Anisotropic re-meshing is used [28, 29] and the mesh refined close to the interfaces as exhibited in Figure 3. With this algorithm, the sizes of the grains at the border of the domain respect the imposed distribution and thus can and are considered in the statistical analysis.

The mesh size in the normal direction is studied in Section 3. The mesh size in the tangential direction as well as far away from the interface (at a distance $\eta = 6.2\mu m$) is fixed at $5\,\mu m$. The initial average grain radius is $\bar{R} \simeq 12\,\mu m$. The average grain boundary energy is aimed at $\bar{\gamma} \simeq 1\,J \cdot m^{-2}$ and the mobility used is $\mu = 0.1\,mm^4 \cdot J^{-1} \cdot s^{-1}$ which are of the order of

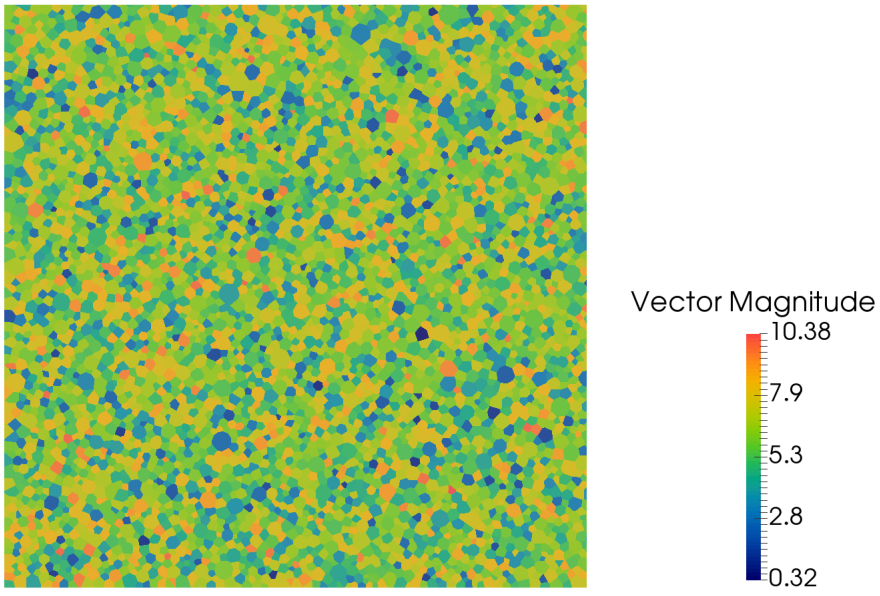

(a) Example of a generated microstructure containing approximately 5000 grains and colored by the magnitude of a vector whose components are the Euler angles of the crystallographic orientations.

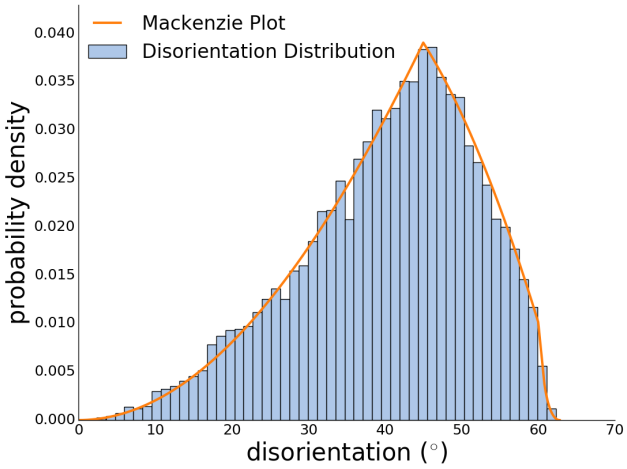

(b) Initial disorientation distribution with the analytical solution for the Mackenzie plot [26]

Figure 2: Crystallographic characterization of the microstructure: (a) an image of the numerical microstructure and (b) its disorientation distribution.

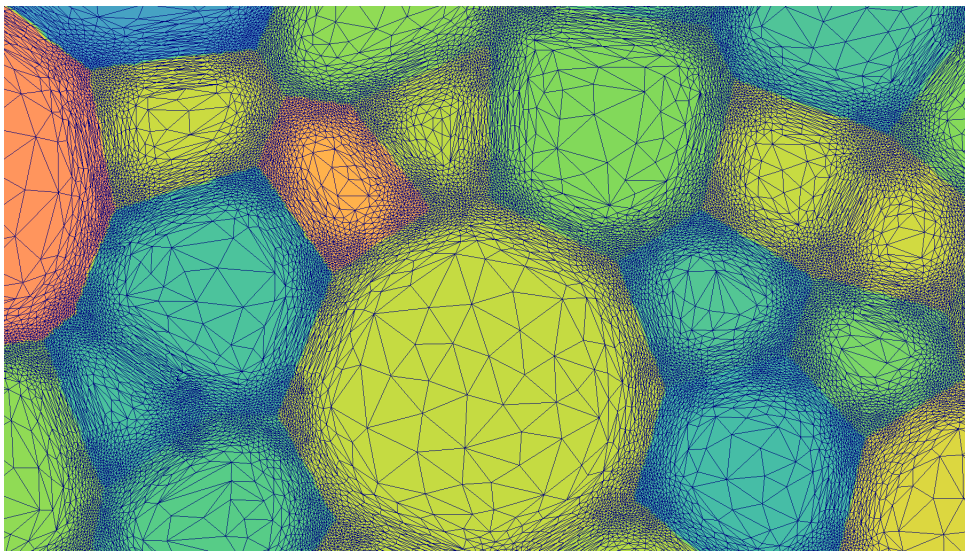

Figure 3: Illustration of the anisotropic mesh refinement operating at the interfaces between grains as in [28, 29], using the same color map as Figure 2a.

pure Nickel at $1400\,K$ [30, 31].

3. Sensitivity analyses

In order to study the sensitivity to numerical parameters in a heterogeneous setting, a form for the misorientation dependent grain boundary energy must be chosen. In the following sections, due to its prevalence in the literature, a Read-Shockley type function (RS) [32] is chosen

$$\gamma(\theta) = \begin{cases} \gamma_{max}\left(\dfrac{\theta}{\theta_{max}}\right)\left(1 - \ln\left(\dfrac{\theta}{\theta_{max}}\right)\right), & \theta < \theta_{max} \\ \gamma_{max}, & \theta \geq \theta_{max} \end{cases} \tag{11}$$

where θ is the disorientation, γ_{max} is the maximal grain boundary energy here equal to $1.012J \cdot m^{-2}$ and θ_{max} is a threshold angle taken here, to be $30°$. Commonly, when using the Read-Shockley function, the low angle grain boundary cut-off is considered to be in the $10-15°$ range. Here, a value of $30°$ was chosen in order to exagerate the heterogeneity and produce measurable heterogeneous effects. The function is plotted in Figure 4.

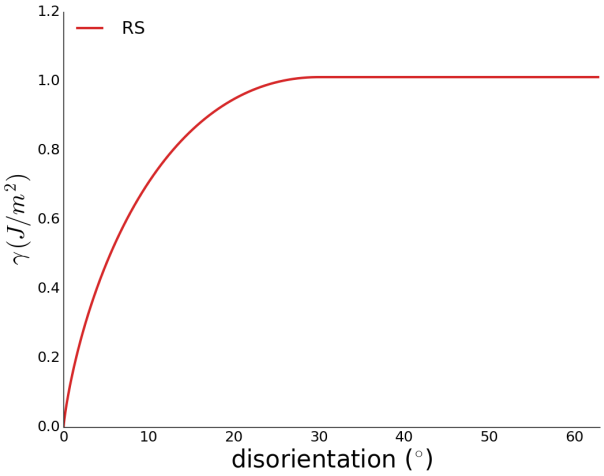

Figure 4: The Read-Shockley (RS) function for grain boundary energy.

The sensitivity of the evolution of the mean grain size $\bar{R}$, the number of grains N_{gr} as well as the total interface energy

$$E_\Gamma = \int_\Gamma \gamma d\Gamma, \tag{12}$$

will be studied. Convergence with regard to a numerical variable x (where x can be the mesh size or the time step) will be determined using an averaged L^2 error e_{L^2} relative to the energy evolution of the microstructure

$$e_{L^2}(x) = \sqrt{\frac{1}{t_{end}} \int_0^{t_{end}} (E_\Gamma^{ref} - E_\Gamma(x))^2 dt}, \tag{13}$$

where E_Γ^{ref} is determined from a linear fit with respect to time of the most precise simulation (i.e. the smallest time step and mesh size). Supposing the evolution of e_{L^2} follows a polynomial type law,

$$e_{L^2}(x) = Ax^n, \tag{14}$$

one may extract the convergence parameters A and n using a logarithmic scale plot.

In order to study the sensitivity of the simulation to the discretization of both space and time a microstructure of physical side length $l = 0.5mm$ was

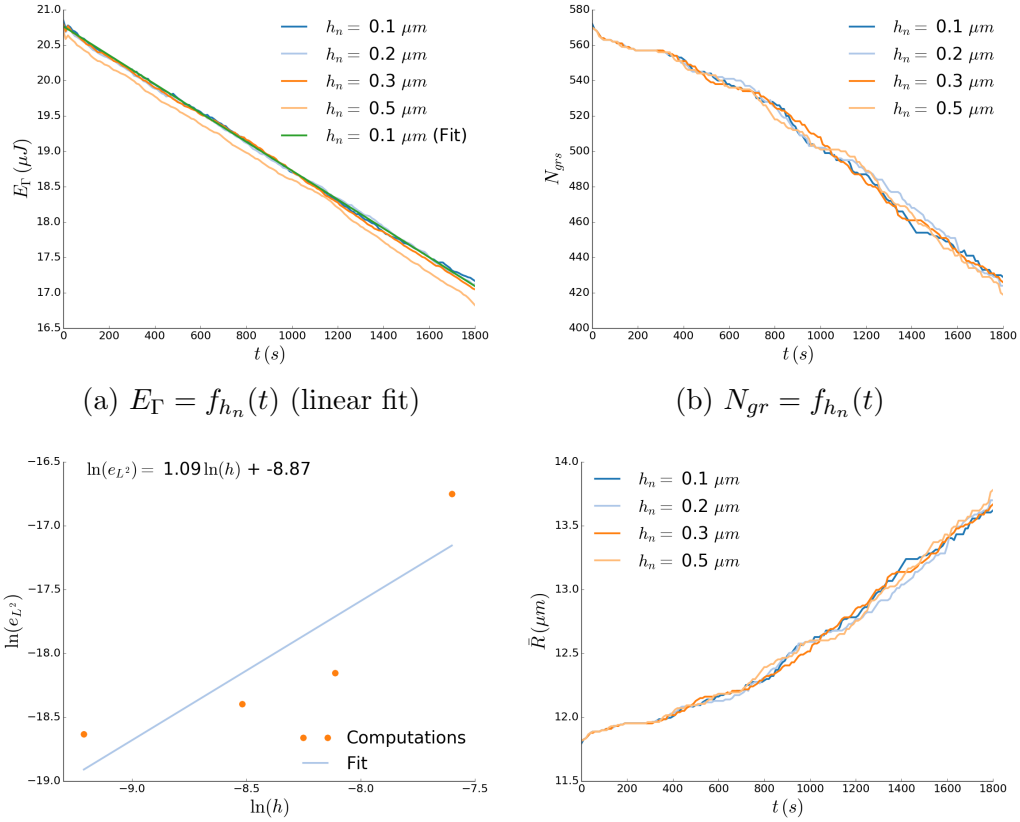

(a) $E_\Gamma = f_{h_n}(t)$ (linear fit)

(b) $N_{gr} = f_{h_n}(t)$

(c) $f(h_n) = e_{L^2}$

(d) $\bar{R} = f_{h_n}(t)$

Figure 5: Evolution of mean field values with the mesh size h_n at a fixed time step $\Delta t = 10s$

generated (containing about 600 grains) and virtually annealed for a physical time of $t_{end} = 30\,min$ with different mesh sizes h_n in mm and time steps Δt in s. The mean value results of these simulations are exposed in Figures 5 and 6 for the mesh size and time step convergence respectively.

Convergence is clearly established both as a function of mesh size and time step for the polycrystal simulations in the range of values presented here. This means that the precision of the solutions obtained can be improved by refining both time and mesh discretizations arbitrarily and independently.

In the calculations that follow, the choice of time step and mesh size will be fixed at $\mathbf{h_n = 0.3\,\mu m}$ and $\mathbf{\Delta t = 10\,s}$.

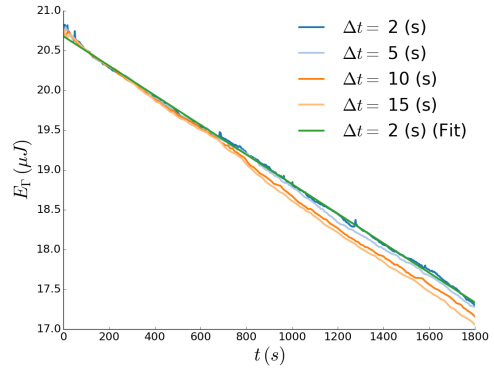

(a) $E_\Gamma = f_{\Delta t}(t)$ (linear fit)

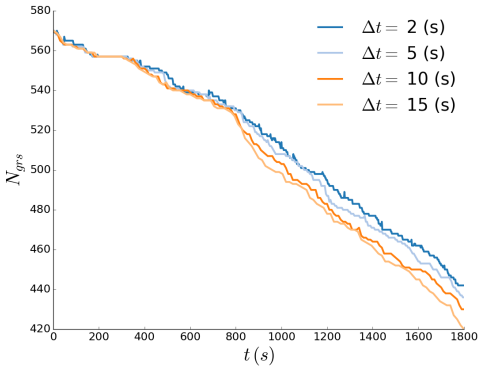

(b) $N_{gr} = f_{\Delta t}(t)$

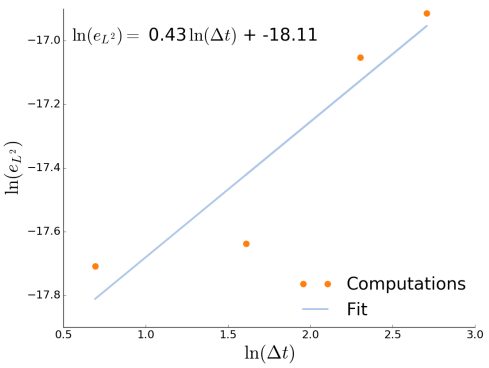

(c) $f(\Delta t) = e_{L^2}$

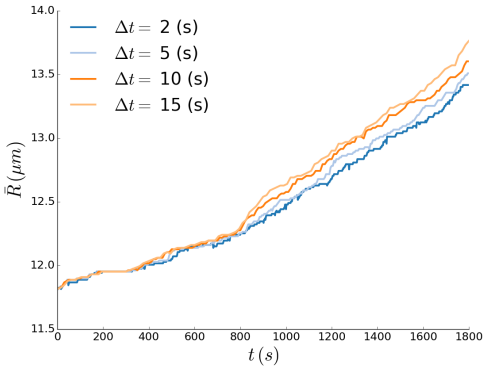

(d) $\bar{R} = f_{\Delta t}(t)$

Figure 6: Evolution of mean field values with the time step Δt at a fixed mesh size $h_n = 0.3\mu m$

4. Various grain boundary energy functions

Even though the RS function for the grain boundary energy is widespread, it does not allow for testing large heterogeneities in untextured microstructures. As such, in order to study the response of a polycrystal to different levels of heterogeneity, grain boundary energy test functions have been generated and compared with respect to the homogeneous case.

Also, one may very well question the statistical representativity of any size microstructure one might chose to simulate [33]. The size of the virtual microstructure determines the population of grain boundaries in the domain and thus whether or not one may consider a given result as representative enough of a given polycrystal behavior. To the authors' knowledge, no such study has been conducted in virtual statistical polycrystal generation such that there is a clear answer as to the number of grain boundaries one might need to simulate in order to obtain trustworthy results in the case of heterogeneous grain boundary energies. As such, in order to circumvent this understandable objection to the results present in this section, the authors propose to only compare microstructural evolutions that originate from exactly the same microstructure. By fixing not only the geometry of the initial grain boundary network but also the orientations of all the grains, the deviations of simulated microstructural evolutions from one another can only be attributed to the differences in their grain boundary energy functions. As such, by comparing any heterogeneous grain boundary energy function to the homogeneous case the simulations may be qualitatively compared so as to infer the effect the heterogeneous grain boundary energy might have on the initial polycrystal. By proceeding in this relative sense the representativity of the microstructure is no longer an issue. In the following, a microstructure with a side length of $\mathbf{1.5mm}$ and approximately 5000 initial grains along with the statistical characteristics described in Section 2 is studied.

4.1. The grain boundary energy functions

In order to compare the effects of different grain boundary energy functions fairly, there must be a common scaling imposed upon the functions such that they become comparable. In this study, an average initial grain boundary energy of the microstructure was imposed constant for all mappings $\gamma(\theta)$:

$$\bar{\gamma} = \frac{\int_\Gamma \gamma d\Gamma}{\int_\Gamma d\Gamma}, \tag{15}$$

which can also be seen as the same initial total energy for all cases given that the initial polycrystal is also unvarying. In order to solve this problem analytically, one can integrate the grain boundary energy function over the disorientation distribution of the microstructure, which is the Mackenzie plot in this case,

$$\bar{\gamma} = \frac{1}{\theta_{lim}} \int_0^{\theta_{lim}} \gamma p_{Mac} d\theta, \tag{16}$$

where p_{Mac} is the probability density related to the Mackenzie distribution [26] and $\theta_{lim} = 62.8$ is the limit of the fundamental region of the disorientation for cubic structures.

Even so, when attempting to choose a misorientation dependent grain boundary energy function there are multiple things one might want to look for. The constant grain boundary energy function, i.e. the homogeneous case, is by default the reference case. The Read-Shockley [32] type grain boundary energy is the most popular function in the current literature for modeling low angle grain boundaries. However, if one wishes to introduce a more diverse set of grain boundaries, one may modify the RS function, for example, in a very discontinuous manner such that the disorientation region where twin boundaries are found can be much lower energy than the rest. Also, in both numerical and experimental approaches to determining the grain boundary energy function, cusps are present and one might wish to study the effect these minima might have on the evolution of the grain boundary network, hence one may use a "bumpy" energy function in order to study these cusps as shown below. In a mathematical approach, one may use a more classical function, such as a Gaussian distribution function, in order to probe the effects of a more "naturally" distributed energy. Given this reasoning, five test functions, which do not aim to be physical representations of the grain boundary energy function, are considered in this work:

Homogeneous

$$\gamma = \bar{\gamma} \tag{17}$$

RS the same as in equation (11).

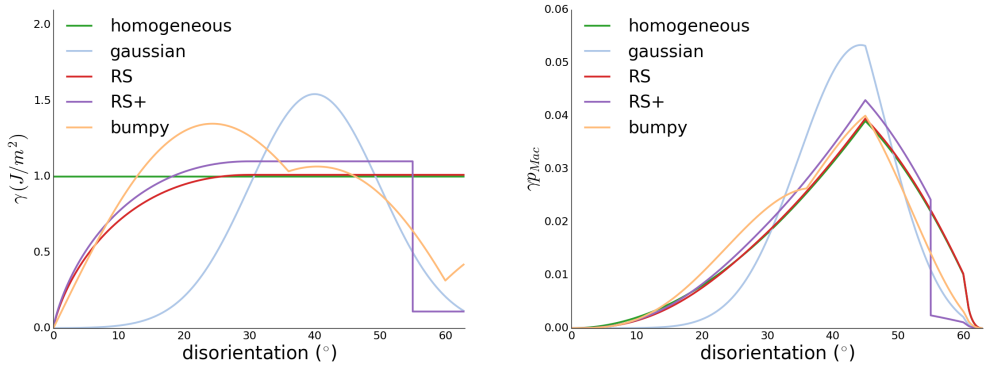

(a) $\gamma(\theta)$ (b) $\gamma p_{Mac}(\theta)$

Figure 7: Considered test grain boundary energy functions.

RS+

$$\gamma = \begin{cases} \gamma_{max}\prime \left(\frac{\theta}{\theta_{max}}\right)\left(1 - \ln\left(\frac{\theta}{\theta_{max}}\right)\right), & \theta < \theta_{max} \\ \gamma_{max}\prime, \quad \theta_{thresh} > \theta > \theta_{max} \\ 0.1\gamma_{max}\prime, \quad \theta > \theta_{thresh} \end{cases}, \tag{18}$$

where $\gamma_{\max}\prime \simeq 1.1\, J/m^2$ and $\theta_{thresh} = 55°$.

Bumpy

$$\gamma = \gamma_b(\alpha_3|\sin(3\theta)| + \alpha_5|\sin(5\theta)|) \tag{19}$$

where $\gamma_b \simeq 1.2\, J/m^2$, $\alpha_3 = 0.9$ and $\alpha_5 = 0.3$.

Gaussian

$$\gamma = \gamma_g e^{\frac{-(\theta-\theta_\mu)^2}{2\theta_\sigma^2}} \tag{20}$$

with $\gamma_g \simeq 1.54 J/m^2$, $\theta_\mu = 40°$ and $\theta_\sigma = 10°$.

Figure 7 shows both the plot of the grain boundary energy functions as well as a graph of the analytical grain boundary energy distribution densities γp_{Mac}.

What is most striking in Figure 7 is that seemingly large differences in the base grain boundary energy functions can actually have little to no impact on the actual heterogeneity present in the microstructure. For example, Figure

Energy Function	d_{L^2}
RS	2.89e-3
RS+	3.70e-2
Bumpy	2.90e-2
Gaussian	6.44e-2

Table 1: The L^2 distances of the heterogeneous γp_{Mac} functions from the homogeneous one.

7b shows that the RS function is actually extremely close to the homogeneous function when the disorientation distribution is taken into account. Even so, the panel of functions chosen here gives access to a relatively diverse spectrum of heterogeneities in the actual microstructure. This can be quantified by the values present in Table 1 which represent the L^2 distance of each of the heterogeneous γp_{Mac} functions with respect to the homogeneous γp_{Mac} function calculated using a simple trapezoidal rule for the numerical integration. This table gives a gauge of the heterogeneities present in each of the functions which can be observed to vary from least to most heterogeneous in the following order: RS, Bumpy, RS+ and Gaussian.

4.2. Evolution of mean field variables

The mean grain size evolution of the homogeneous case is fitted with a generalized Burke and Turnbull type law [3, 34].

The first observation concerning the time evolution of both the mean grain radius and the number of grains is that the more heterogeneous a grain boundary energy function is, the slower its kinetics, a result easily corroborated in most heterogeneous grain growth simulations in the literature [6–11, 14, 15]. Looking at the evolution of the energy however, the cases with the most heterogeneity are also those which dissipate the interface energy the most efficiently. As such, the most heterogeneous case should have the smallest grains and thus the largest amount of interface length and yet it has the smallest total energy. A direct explanation for this phenomenon could be that the most heterogeneous cases have the most diverse grain boundary energy distributions and thus the most degrees of freedom for minimizing the energy of the system.

Also, the slowing of the kinetics of grain growth could be related to the phenomenon discussed in certain experimental studies known as orientation

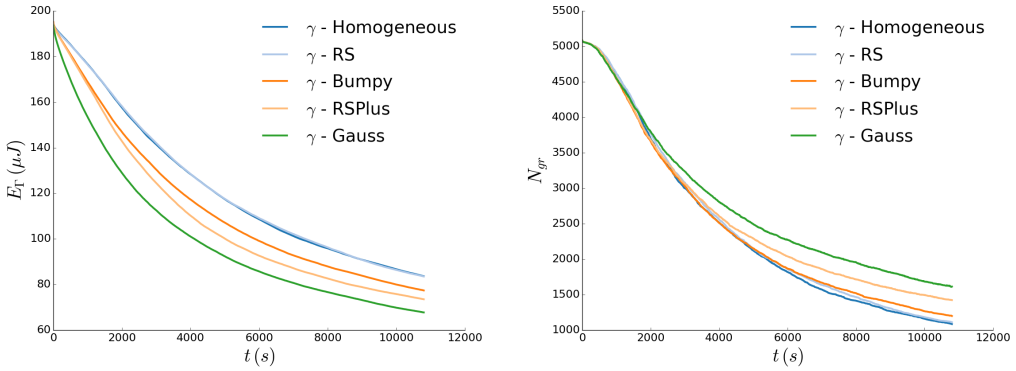

(a) $E_\Gamma = f(t)$ (b) $N_{gr} = f(t)$

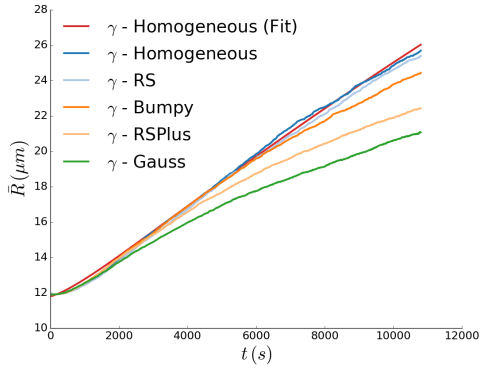

(c) $\bar{R} = f(t)$

Figure 8: Time evolution of mean values for the different grain boundary energy functions.

pinning [35, 36]. This mechanism is related to the fact that as grains grow and compete for space, the probability that a grain encounters a particularly unfavorable orientation for its continued expansion increases. As the grain meets this disadvantageous orientation (creating a low energy grain boundary) its kinetics slow and therefore the orientation cohabitation tends to persist during the rest of the grain coarsening process. Typically, this is a process that is not observable in simulations unless using a heterogeneous description of the grain boundary energy and becomes even more evident as the heterogeneity is increased.

More generally, the results presented in Figure 8 show that even with the same average grain boundary energy, the kinetics of grain growth can vary significantly. As such, using time evolution of grain size, for example, in order to calibrate average grain boundary energies experimentally is clearly limited. More in depth characterizations of the microstructure are needed in order to probe the nature of the grain boundary energy distribution. In [37] is proposed an interesting idea in which the grain boundary character distribution should be inversely correlated to the grain boundary energy function. In other terms, the most energetic grain boundaries should tend to disappear leaving only the least energetic boundaries during grain growth.

4.3. Grain boundary network characterizations

In a three dimensional experimental polycrystal, the grain boundary character distribution would have to be set in the five dimensional grain boundary space [38] in order to be complete. However, this is impractical due to the high dimensionality and small datasets available. In this work, given the way in which the grain boundary energy functions are defined, only one variable of the grain boundary character is considered, the disorientation. As such, the disorientation distributions at $10000\,s$ are plotted for the different grain boundary energy functions as well as the grain boundary energy distributions in Figure 9. The grain size distributions are also compared in the same figure.

The differences in between the disorientation distributions obtained from the different grain boundary energy functions are striking. While the homogeneous case emulates the Mackenzie plot throughout the simulation, the RS function, even given its proximity to the homogeneous case, favors low angle grain boundaries, a result also found in [6, 12, 13]. The RS+ case also encourages low angle grain boundaries, as in the RS case, but tilts towards the high angle boundaries as well (the transition is around $55°$). The bumpy

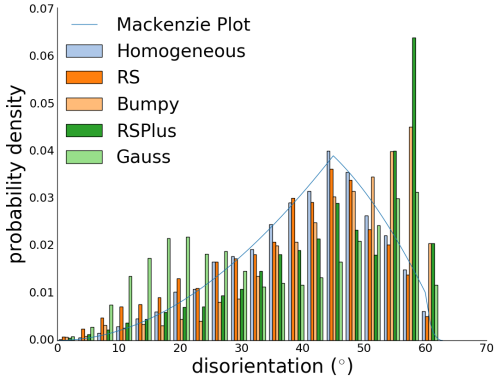

(a) Normalized grain boundary disorientation distribution

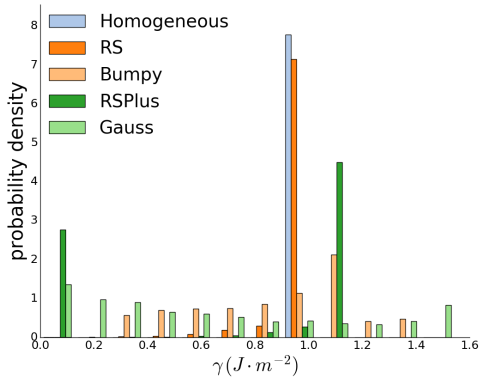

(b) Normalized grain boundary energy distribution

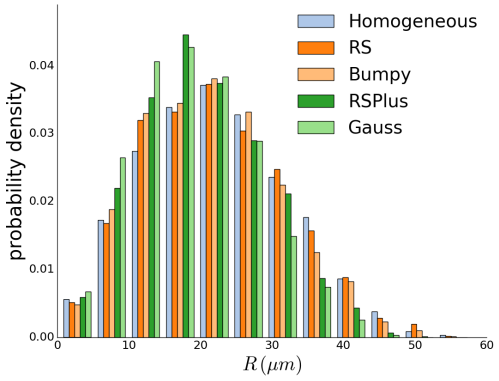

(c) Normalized grain size distribution (in number)

Figure 9: Comparisons of the different grain boundary energy functions using various distributions after 10000 s of numerical annealing.

case also tends toward keeping its least energetic boundaries, a behavior replicated in the gaussian case which tilts towards a bimodal distribution. Globally, using this formulation for grain growth, the character distribution of the boundaries are clearly inversely correlated with the grain boundary energy functions, a statement also supported by the grain boundary energy distributions, which would corroborate [37].

The grain size distributions are relatively diverse as well. However, upon closer inspection, they all respect a lognormal type distribution law and their differences can be clearly explained by the different growth kinetics of the different cases shown in Figure 8.

The virtual micrographs of the various cases after 3 hours of annealing are presented in Figure 10. The quantitative results present in Figure 9 are clearly represented in the virtual microstructures qualitatively given the diversity of grain boundary energies. Perhaps more interestingly however, the grain boundary energy landscape is not the only observable difference in between the grain boundary networks developed using different grain boundary energy functions. The morphology of the grains in different cases are also relatively varied. While the least heterogeneous cases tend to favor relatively regular polyhedra, the most heterogeneous cases seem to develop more rectangular and disparate grains. This observation can be made more quantitative with the introduction of Figure 11. The distributions of the number of neighboring grains for each grain boundary energy functions remain centered around 5 and 6. However, the more heterogeneous cases tend to flatten their distributions acquiring a greater zoology of grains than in the more homogeneous cases, a result corroborated by [8] but contested by [10]. This polycrystal behavior is most likely a product of the diversity of triple junctions in the most heterogeneous cases compared to the more homogeneous ones. Indeed, as more and more triple junctions stray from the homogeneous 120° angle equilibrium, the forms of the grains become more irregular and the polycrystal manages to obtain a more diverse set.

Conclusion

A sensitivity analysis to multiple numerical parameters for the simulation of grain coarsening has been performed for heterogeneous grain boundary energy microstructures. The response of the grain coarsening simulation was then studied for different grain boundary energy functions and it was found that:

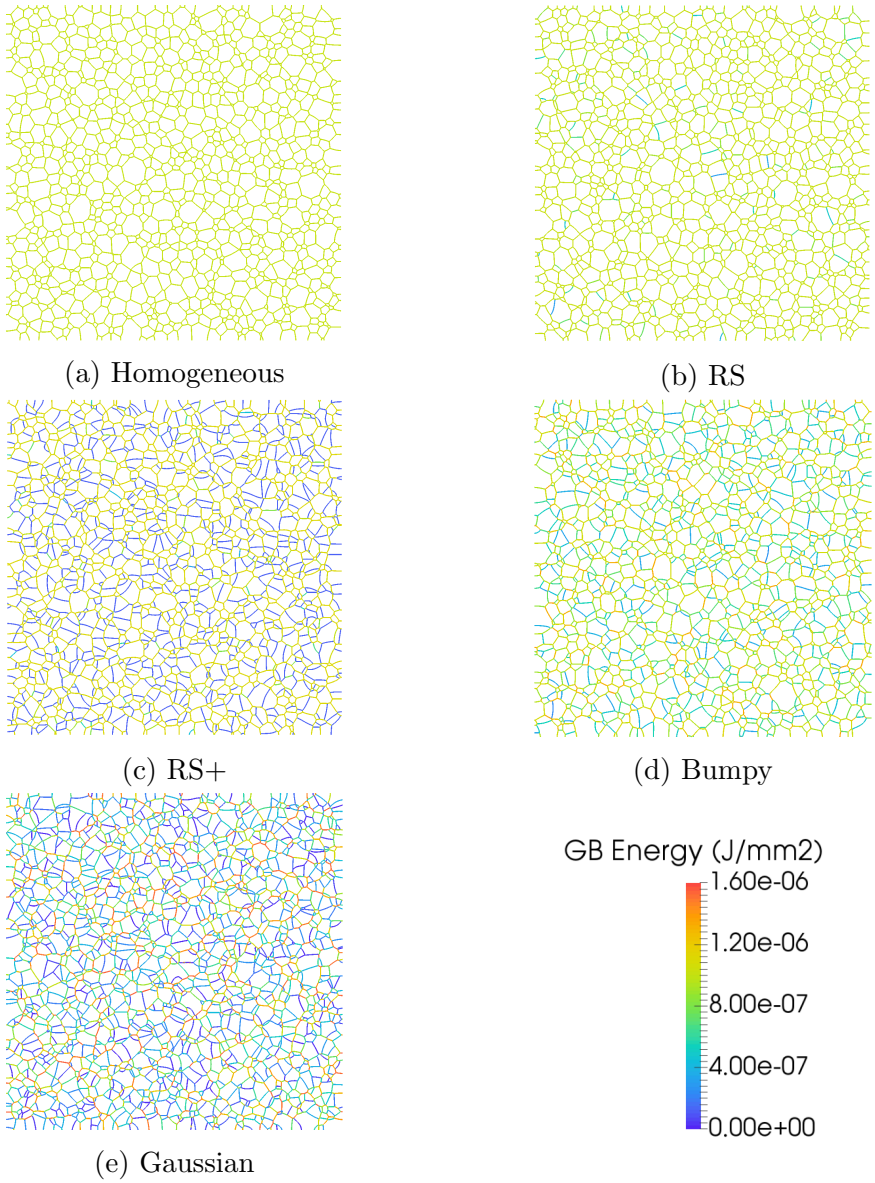

(a) Homogeneous

(b) RS

(c) RS+

(d) Bumpy

(e) Gaussian

Figure 10: States of grain boundary networks obtained for all grain boundary energy functions after 3 hours of numerical heat treatment.

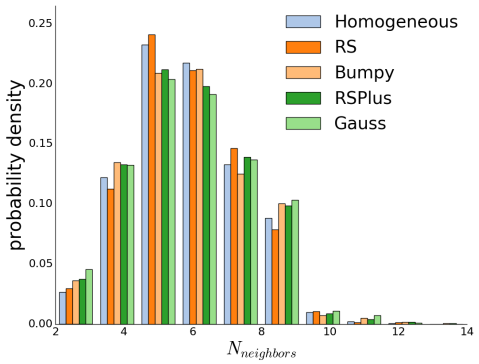

Figure 11: Normalized number of neighboring grains distributions for all of the studied grain boundary energy functions at 10000 s.

- the kinetics of grain growth are slower for more heterogeneous grain boundary energy functions, similar to the findings in other works [6–11, 14, 15],
- the disorientation distributions are clearly inversely correlated to the grain boundary energy functions as predicted in [37],
- and the morphology of the grains are also heavily dependent upon the grain boundary energy function used in the simulation of grain growth.

With the authors' present knowledge of the heterogeneous grain growth literature, no other study has compared the effects of grain boundary energy functions on grain growth using such a diverse set.

A serious limitation to the application of these results to experimental works is the 2D nature of the simulations. However, the mathematical formulation is dimension independent and 3D calculations are forthcoming. Different misorientation dependent grain boundary energy functions have been proposed in the literature [39, 40], and their testing and comparison with experimental results is a perspective of this study. Also, the dependence of the grain boundary energy to the inclination of the boundary as well as the misorientation rotation axis were conveniently ignored in this work and their integration is a perspective non-trivial step in the continuation of the framework's development. For example, the torque terms generated by inclination dependent grain boundary energies cannot be simply expressed by the contraction of gradient of the grain boundary energy function $\nabla\gamma$ on the

normal **n** given the tangentiality of this gradient field to the grain boundary surface far away from boundary junctions. As such, new supplemental terms depending both on γ and the geometry of the boundary must be developed and integrated in order to aspire to a fully anisotropic formulation for grain growth.

Acknowledgements

The authors thank the group SAFRAN and the ANR (French National Research Agency) for their financial support through the OPALE industrial ANR chair.

Data Availability

The raw and processed data required to reproduce these findings cannot be shared at this time as the data also forms part of an ongoing study.

References

[1] H. Hallberg, Approaches to modeling of recrystallization, Metals 1 (1) (2011) 16–48. doi:10.3390/met1010016.
URL http://www.mdpi.com/2075-4701/1/1/16

[2] M. Bernacki, R. Logé, T. Coupez, Level set framework for the finite-element modelling of recrystallization and grain growth in polycrystalline materials, Scripta Materialia 64 (2011) 525–528.

[3] A. L. Cruz-Fabiano, R. E. Logé, M. Bernacki, Assessement of simplified 2d grain growth models from numerical experiments based on a level set framework, Computational Materials Science 92 (2014) 305–312.

[4] L. Maire, B. Scholtes, C. Moussa, N. Bozzolo, D. Pino Muñoz, M. Bernacki, Improvement of 3d mean field models for capillarity-driven grain growth based on full field simulations, Journal of Materials Science 51 (24) (2016) 10970–10981. doi:10.1007/s10853-016-0309-6.
URL https://doi.org/10.1007/s10853-016-0309-6

[5] M. Elsey, S. Esedolu, P. Smereka, Large-scale simulation of normal grain growth via diffusion-generated motion, Proceedings of the Royal Society A: Mathematical, Physical and Engineering Sciences 467 (2126) (2011) 381–401. doi:10.1098/rspa.2010.0194.

[6] E. Miyoshi, T. Takaki, Multi-phase-field study of the effects of anisotropic grain-boundary properties on polycrystalline grain growth, Journal of Crystal Growth 474 (2017) 160–165.

[7] K. Chang, L.-Q. Chen, C. E. Krill, N. Moelans, Effect of strong nonuniformity in grain boundary energy on 3-d grain growth behavior: A phase-field simulation study, Computational Materials Science 127 (2017) 67–77.

[8] K. Chang, N. Moelans, Effect of grain boundary energy anisotropy on highly textured grain structures studied by phase-field simulations, Acta Materialia 64 (2014) 443–454.

[9] M. A. Zaeem, H. E. Kadiri, P. Wang, M. Horstemeyer, Investigating the effects of grain boundary energy anisotropy and second-phase particles on grain growth using a phase-field model, Computational Materials Science 50 (2011) 2488–2492.

[10] A. Mallick, S. Vedantam, Phase field study of the effect of grain boundary energy anisotropy on grain growth, Computational Materials Science 46 (2009) 21–25.

[11] Y. Jin, N. Bozzolo, A. D. Rollett, M. Bernacki, 2d finite element modeling of misorientation dependent anisotropic grain growth in polycrystalline materials: Level set versus multi-phase-field method, Computational Materials Science 104 (2015) 108–123.

[12] H. Hallberg, Influence of anisotropic grain boundary properties on the evolution of grain boundary character distribution during grain growth - a 2d level set study, Modelling and Simulation in Materials Science and Engineering 22 (8) (2014) 085005.
URL `http://stacks.iop.org/0965-0393/22/i=8/a=085005`

[13] M. Elsey, S. Esedoglu, P. Smereka, Simulations of anisotropic grain growth: Efficient algorithms and misorientation distributions, Acta Materialia 61 (2013) 2033–2043.

[14] Q. Yu, M. Nosonovsky, S. K. Esche, Monte carlo simulation of grain growth of single-phase systems with anisotropic boundary energies, International Journal of Mechanical Sciences 51 (2009) 434–442.

[15] G. S. Grest, D. J. Srolovitz, M. P. Anderson, Computer simulation of grain growth - iv. anisotropic grain boundary energies, Acta Metallurgica 33 (1985) 509–520.

[16] H. Hallberg, V. V. Bulatov, , Modelling and Simulation in Materials Science and Engineering 27 (4) (2019) 045002. doi:10.1088/1361-651x/ab0c6c.
URL

[17] E. Miyoshi, T. Takaki, Validation of a novel higher-order multi-phase-field model for grain-growth simulations using anisotropic grain-boundary properties, Computational Materials Science 112 (2016) 44 – 51. doi:https://doi.org/10.1016/j.commatsci.2015.10.010.
URL http://www.sciencedirect.com/science/article/pii/S0927025615006576

[18] J. Fausty, D. Pino Muñoz, N. Bozzolo, M. Bernacki, A novel level-set finite element formultion for grain growth with heterogeneous grain boundary energies, Materials and Design 160 (2018) 578–590.

[19] S. K. Behera, Kinetics of grain growth in la-doped ultrapure al2o3, Journal of Alloys and Compounds 683 (2016) 444 – 449. doi:https://doi.org/10.1016/j.jallcom.2016.05.109.
URL http://www.sciencedirect.com/science/article/pii/S0925838816314426

[20] F. Humphreys, M. Hatherly, Recrystallization and Related Annealing Phenomena, Elsevier Science, 2012.
URL https://books.google.fr/books?id=Kt11V4m2bqEC

[21] J. A. Sethian, Theory, algorithms, and applications of level set methods for propagating interfaces, Acta Numerica 5 (1996) 309395. doi:10.1017/S0962492900002671.

[22] B. Merriman, J. K. Bence, S. J. Osher, Motion of multiple junctions: A level set approach, Journal of Computational Physics 112 (1994) 334–363.

[23] M. Shakoor, B. Scholtes, P.-O. Bouchard, M. Bernacki, An efficient and parallel level set reinitialization method - application to micromechanics and microstructural evolutions, Applied Mathematical Modelling 39 (2015) 7291–7302.

[24] A. N. Brooks, A Petrov-Galerkin finite element formulation for convection dominated flows, Ph.D. thesis, California Institute of Technology (1981).

[25] C. Geuzaine, J.-F. Remacle, Gmsh: A 3-d finite element mesh generator with built-in pre- and post-processing facilities, International Journal for Numerical Methods in Engineering 79 (11) (2009) 1309–1331. arXiv:https://onlinelibrary.wiley.com/doi/pdf/10.1002/nme.2579, doi:10.1002/nme.2579.
URL https://onlinelibrary.wiley.com/doi/abs/10.1002/nme.2579

[26] J. K. Mackenzie, Second paper on statistics associated with the random disorientation of cubes, Biometrika 45 (1958) 229–240.

[27] K. Hitti, P. Laure, T. Coupez, L. Silva, M. Bernacki, Precise generation of complex statistical Representative Volume Elements (RVEs) in a finite element context, Computational Materials Science 61 (2012) 224–238.

[28] B. Scholtes, M. Shakoor, A. Settefrati, P.-O. Bouchard, N. Bozzolo, M. Bernacki, New finite element developments for the full field modeling of microstructural evolutions using the level-set method, Computational Materials Science 109 (2015) 388–398.

[29] E. Roux, M. Bernacki, P. Bouchard, A level-set and anisotropic adaptive remeshing strategy for the modeling of void growth under large plastic strain, Computational Materials Science 68 (2013) 32–46.

[30] D. L. Olmsted, S. M. Foiles, E. A. Holm, Survey of computed grain boundary properties in face-centered cubic metals: I. Grain boundary energy, Acta Materialia 57 (2009) 3694–3703.

[31] D. L. Olmsted, S. M. Foiles, E. A. Holm, Survey of computed grain boundary properties in face-centered cubic metals: II. Grain boundary mobility, Acta Materialia 57 (2009) 3704–3713.

[32] W. T. Read, W. Shockley, Dislocation models of crystal grain boundaries, Physical Review 78 (1950) 275–289.

[33] L. Madej, Digital/virtual microstructures in application to metals engineering a review, Archives of Civil and Mechanical Engineering

17 (4) (2017) 839 – 854. doi:https://doi.org/10.1016/j.acme.2017.03.002.
URL http://www.sciencedirect.com/science/article/pii/S1644966517300328

[34] J. Burke, D. Turnbull, Recrystallization and grain growth, Progress in Metal Physics 3 (1952) 220 – 292. doi:https://doi.org/10.1016/0502-8205(52)90009-9.
URL http://www.sciencedirect.com/science/article/pii/0502820552900099

[35] S. Takajo, C. Merriman, S. Vogel, D. Field, In-situ EBSD study on the cube texture evolution in 3wt% si steel complemented by ex-situ EBSD experiment From nucleation to grain growth, Acta Materialiadoi:https://doi.org/10.1016/j.actamat.2018.11.054.
URL http://www.sciencedirect.com/science/article/pii/S1359645418309315

[36] O. Engler, On the influence of orientation pinning on growth selection of recrystallisation, Acta Materialia 46 (5) (1998) 1555 – 1568. doi:https://doi.org/10.1016/S1359-6454(97)00354-6.
URL http://www.sciencedirect.com/science/article/pii/S1359645497003546

[37] E. A. Holm, G. S. Rohrer, S. M. Foiles, A. D. Rollett, H. M. Miller, D. L. Olmsted, Validating computed grain boundary energies in fcc metals using the grain boundary character distribution, Acta Materialia 59 (2011) 5250–5256.

[38] A. Sutton, R. Ballufi, Interfaces in crystalline materials, Clarendon Press, 1995.

[39] D. Wolf, Correlation between energy and volume expansion for grain boundaries in fcc metals, Scripta Metallurgica 23 (11) (1989) 1913 – 1918. doi:https://doi.org/10.1016/0036-9748(89)90482-1.
URL http://www.sciencedirect.com/science/article/pii/0036974889904821

[40] V. V. Bulatov, B. W. Reed, M. Kumar, Grain boundary energy function for fcc metals, Acta Materialia 65 (2014) 161 – 175. doi:https://doi.org/10.1016/j.actamat.2013.10.057.
URL http://www.sciencedirect.com/science/article/pii/S1359645413008203